IMECE2020-24646

A COMPARISON OF SMOOTHED PARTICLE HYDRODYNAMICS (SPH) AND COUPLED SPH-FEM METHODS FOR MODELING MACHINING

Nishant Ojal*and Harish P. Cherukuri
Department of Mechanical Engineering and Engineering Science
The University of North Carolina at Charlotte,
Charlotte, NC 28223-0001
Email: nojal@uncc.edu

Tony L. Schmitz
ORNL Joint Faculty
Mechanical, Aerospace, and Biomedical Engineering
The University of Tennessee, Knoxville
Knoxville, TN 37996-2210.
Adam W. Jaycox
Lawrence Livermore National Laboratory
Livermore, CA 94550.

ABSTRACT

Smoothed Particle Hydrodynamics (SPH), a particle-based, meshless method originally developed for modeling astrophysical problems, is being increasingly used for modeling fluid mechanics and solid mechanics problems. Due to its advantages over grid-based methods in handling of large deformations and crack formation, SPH method is increasingly being applied to model material removal processes. However, SPH method is computationally expensive. One way to reduce the computational time is to partition the domain into two parts, where in one segment undergoing large deformations and material separation, the SPH method is used and in the second segment, the conventional finite element (FE) mesh is used.

In this work, the accuracy of this approach is investigated in the context of orthogonal cutting. The high deformation zone (where chips form and curl) is meshed with the SPH method, while the rest of the workpiece is modeled using the FE method. At the interface, SPH particles are coupled with FE mesh for smooth transfer of stress and displacement. The boundary conditions are applied to tool and FE zone of the workpiece. First, the SPH model (workpiece fully discretized by SPH) is validated. This is followed by a comparison of the results from the coupled SPH-FE model with the SPH model. The coupled SPH-FE model is developed using the same material parameters and ma-chining conditions. A comparison of the chip profile, the cutting force, the von Mises stress and the damage parameter show that the coupled SPH-FE model reproduces the SPH model results accurately. However, the SPH-FE model takes almost 40% less time to run, a significant gain over the SPH model. Similar reduction in computation time is observed for the micro-cutting application (depth of cut of 300 nm). Based on these results, it is concluded that coupling SPH with FEM in machining models decreases simulation time significantly while producing accurate results. This becomes more significant for the modeling three-dimensional machining problems efficiently.

INTRODUCTION

The finite element method is the most commonly used method for modeling machining processes. However, the method suffers from several drawbacks depending on the approach used: Lagrangian, Eulerian or Arbitrary Lagrangian-Eulerian (ALE) formulations. In the Lagrangian formulation [1], the mesh is fixed to the geometry and therefore, severe mesh distortion is an issue. A work-around is to use the element deletion technique which leads to the problem of mass loss. In the Eulerian formulation [2], the mesh is fixed in space and thus requires an advance knowledge of chip geometry. The ALE formulation [3] incorporates the benefits of both the approaches, but requires frequent remeshing in the high deformation zones and hence, high compu-

---

*Address all correspondence to this author.

tational cost. Another challenge with these methods is the need to prescribe, a priori, the path of failure to model chip separation.

Due to these disadvantages, the smoothed particle hydro-dynamics method (SPH), originally developed in the late 1970s for modeling astrophysical problems [4], has attracted the attention of many researchers as an alternative to the finite element method. The SPH method is a Lagrangian, particle-based, mesh-less method that has several advantages over the grid-based approaches. High strains occurring in machining are easily modeled due to the meshless nature of the method. Particles undergoing deformation move without any topological restrictions. Furthermore, a separation model or contact model is not required in the SPH method with the relative motion of the particles with respect to each other and with respect to the tool surface creating a "natural" chip-workpiece separation.

A drawback of SPH however is that the computational time for simulations depends on the number of particles in the support domain, discussed in more detail in a later section, of each particle. The higher the number of particles in this domain, the longer the job takes to run. This can be a severe impediment to considering realistic models of a machining process and obtaining accurate results. To address this concern, in the present work, a coupled SPH-FE model is proposed where the SPH model is used for the region where severe deformations and material removal takes place and the FE model is used for the rest of the workpiece. The results from this model are compared with a validated fully-SPH model. Based on the comparisons, it is concluded the combined SPH-FE model predicts essentially the same results as the SPH model while taking significantly less time to run.

In the following, the methodology and the results used to reach this prediction are presented along with a brief overview of some of the prior work in the SPH modeling of metal cutting.

1 Prior SPH Studies of Cutting

Orthogonal machining using SPH has been studied by various researchers. Limido et al. [5] compared the 2D orthogonal machining SPH model for machining with commercial package AdvantEdge and experiments to study the advantages of SPH, namely meshless nature for handing high strains, chip workpiece separation and modeling of friction as particle interaction. Chip morphology and cutting forces are the validation criteria. The SPH model is able to predict continuous and shear localized chips and all the steps of its formation. The cutting forces agree within 10% and 30% of the measured values for tangential and normal components respectively.

Espinosa et al. [6] modeled 2D orthogonal cutting and 3D oblique cutting models using SPH. The comparison of chip morphology and cutting forces with experiments was done. Also, some specific aspects of implementation of SPH in LS-DYNA is provided. For example, artificial viscosity (they observed

smoothness of von Mises stress when the default value of Q2 was changed to 0.5), use of renormalized formulation (observed more realistic modeling of chip curve) and observation of numerical instability (taken care by increasing the tool velocity by ten times).

Schwer [7] has some important notes regarding artificial viscosity and Johnson Cook failure model in SPH simulations. He stated that he was informed by Lacome (developer of SPH in LS-DYNA) that the linear viscosity coefficient Q2 should be increased from default 0.06 to 1.00. But in absence of Johnson Cook failure model led to decrease in average particle residual speed to a very low value as compared to experiments. Upon inclusion of the failure criteria, the speed was comparable to the experiments. This can be a "calibration" parameter of a model to obtain better agreement with experimental observations.

Villumsen et al. [8] developed 3D orthogonal cutting model of AL 6082-T6 in LS-DYNA using SPH. Detailed set-up of model in LS-DYNA is provided in the paper. Sensitivity analysis to evaluate the model is performed. SPH parameters, namely particle resolution (observed affecting convergence of result), mass scaling (concluded as not an adequate way to reduce calculation time), process time scaling (concluded as effective with reasonable assumption for analysis) and friction (observed that force curves have increasing tendency with increase in friction) significantly affected force output. Little or no effect on force output is reported by the changing the parameters like MEMORY on the *CONTROL SPH card, CLSH on *SECTION SPH card, interval between data written to RCFORCE file and penalty and soft contact formulation. Chip formation and obtained force output is found to be in good agreement with the experimental results.

Avachat et al. [9] investigated orthogonal machining of AISI 1045 with the focus on the effect of the three most important parameters, namely, the smoothing length, particle density and SPH formulation on chip morphology and stress distribution.The sensitivity of chip morphology and stresses to Johnson-Cook parameters for AISI 1045 steel is also investigated.

Madaj et al. [10] performed orthogonal simulations of A2024-T351 alloy using SPH. They observed that chip segmentation can be controlled by setting the Johnson-Cook failure parameters (D1-D5 values) and EFMIN value (the minimum required strain for failure or the lower bound for strain at fracture). They evaluated the effect of friction on cutting forces and concluded that higher friction coefficient led to the higher chip radius, lower shear plane angle and thicker chip, higher plastic strain values and higher average cutting force. They noted the need for investigation of material models to examine their usability for SPH simulations.

Xi et al. [11] developed machining models to study the thermally assisted machining of Ti6Al4V and studied the influence of the initial workpiece temperature on the chip formation and cutting force. To reduce the computation time, the coupled SPH-FE model was developed with workpiece discritized by SPH particles near the tool (high deformation zone) and meshed by FE mesh away from the tool. Chip segmentation and cyclic cutting force was observed.

2 Smoothed Particle Hydrodynamics (SPH) method

Smoothed particle hydrodynamics (SPH) is a meshfree, Langrangian method introduced by Gingold and Monaghan [4] and Lucy in 1977 for astrophysical applications. However, due to its advantages, the method being increasingly used solid and fluid mechanics. In this method, the body is discretized into particles. Each particle has a set of state variables associated with them. The particle interacts with the neighboring particles which are within its domain of influence (support domain). Smoothing or kernel functions provide the weighted contributions from the neighboring particles to the state variables associated with each particle at any instant of time. The discretized conservation equations along with constitutive equations are solved to obtain the time variation of the state variables. The method is described in detail in [12], [13].

At the core of the SPH method is the smoothing function or kernel function. The kernel function smoothes out the neighbouring particle's contribution to a property field based on distance from the respective particle. The influences of the neighbouring particle reduces with the increasing distance. The summation form of a property field f at position $\mathbf{r}^a$ is given by

$$\langle f(\mathbf{r}^a) \rangle = \sum_{b=1}^{N} W(\mathbf{r}^{ab}, h) f(\mathbf{r}^b) \frac{m^b}{\rho^b} . \tag{1}$$

Here, $W(\mathbf{r}^{ab}, h)$ is the smoothing function, $\mathbf{r}^{ab} = |\mathbf{r}^a - \mathbf{r}^b|$ is the distance of neighbouring particle at position $\mathbf{r}^b$ from the particle at $\mathbf{r}^a$, h is called smoothing length, ρ is the density of particle and m is the mass of the particle. Clearly, Eqn. (1) calculates the value of a property at a point using the summation of the values of the property at the neighbouring particles, weighted by the kernel function, as illustrated in Fig. 1.

2.1 Discrete form of Conservation laws

The conservation laws are discretized using Eqn. (1). For example, the conservation of mass in summation approximation
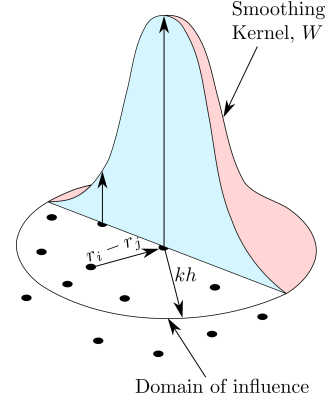
FIGURE 1. A schematic of a smoothing kernel function.

is written as,

$$< \frac{D\rho^a}{Dt} > = \sum_{b=1}^{N} m^b \left(v_i^a - v_i^b \right) \frac{\partial W^{ab}}{\partial x_i^a} . \tag{2}$$

Here, ρ is the density, m is mass, $\mathbf{v}$ is velocity and x_i are the coordinates. The evolution of density is governed by this equation.

Similarly, the conservation of linear momentum is written as,

$$< \frac{Dv_i^a}{Dt} > = \sum_{b=1}^{N} m^b \left(\frac{\sigma_{ij}^a}{(\rho^a)^2} + \frac{\sigma_{ij}^b}{(\rho^b)^2} - \Pi_{ij} \right) \frac{\partial W^{ab}}{\partial x_j^a} . \tag{3}$$

Here, σ is the total stress tensor and Π_{ij} is the artificial viscosity term accounting for numerical instability during discontinuity, for example shock. The equation of conservation of linear momentum evolves the forces on the particles during the simulation. The conservation of angular momentum is satisfied explicitly by the SPH formulation.

The conservation of energy is written as,

$$< \frac{DU^a}{Dt} > = \frac{1}{2} \sum_{b=1}^{N} m^b \left(\frac{p^a}{(\rho^a)^2} + \frac{p^b}{(\rho^b)^2} \right) v_j^{ab} \frac{\partial W^{ab}}{\partial r_j^a} + \frac{\mu^a}{2\rho^a} \varepsilon_{ij}^a \varepsilon_{ij}^a . \tag{4}$$

Here, U is internal energy per unit mass, p is isotropic pressure component of the total stress tensor σ, μ is dynamic viscosity, and ε is the shear strain rate.

2.2 Equation of state

The equation of state (EOS) determines pressure p as a function of local density ρ and other material property variables. For machining simulations, Mie-Grüneisen equation has been widely

used and is given by the following equations. For compression, $(\mu > 0)$,

$$p = \frac{\rho_0 C^2 \mu \left[1 + \left(1 - \frac{\gamma_0}{2}\right)\mu - \frac{b}{2}\mu^2\right]}{\left[1 - (S_1 - 1)\mu - S_2\frac{\mu^2}{\mu+1} - S_3\frac{\mu^3}{(\mu+1)^2}\right]^2} + (\gamma_0 + b\mu)e , \quad (5)$$

and for tension, $(\mu < 0)$,

$$p = \rho_0 C^2 \mu + (\gamma_0 + b\mu)e . \quad (6)$$

Here, C is the bulk speed of sound, $\mu = \rho/\rho_0 - 1$, ρ is current density, ρ_0 is reference density, γ_0 is Grüneisen gamma, S_1, S_2 and S_3 are Hugoniot slope coefficients, b is the first order volume correction to γ_0 and e is the internal energy per initial volume. The parameters $C, \gamma_0, S_1, S_2, S_3$ and b define EOS of the material.

2.3 Material model

The total stress tensor σ consists of the hydrostatic pressure p and the deviatoric stress $\mathbf{S}$, given, in component form, by,

$$\sigma_{ij} = -p\delta_{ij} + S_{ij} . \quad (7)$$

The deviatoric stress is evolved using Jaumann rate and is expressed as,

$$\dot{S}_{ij} = 2G\left(d_{ij} - \frac{\delta_{ij}d_{kk}}{3}\right) + S_{ik}w_{jk} + S_{jk}w_{ik} . \quad (8)$$

Here, G is shear modulus, d is strain rate tensor and w is rotation tensor given by,

$$d_{ij} = \frac{1}{2}\left(\frac{\partial v_i}{\partial x_j} + \frac{\partial v_j}{\partial x_i}\right), \quad w_{ij} = \frac{1}{2}\left(\frac{\partial v_i}{\partial x_j} - \frac{\partial v_j}{\partial x_i}\right) . \quad (9)$$

The inelastic behaviour of the workpiece is modelled using the Johnson-Cook material model given by,

$$\sigma_{eq} = \underbrace{(A + B\varepsilon_p^n)}_{\text{Strain hardening}} \underbrace{\left[1 + C\log\left(\frac{\dot{\varepsilon}_p}{\dot{\varepsilon}_0}\right)\right]}_{\text{Strain rate sensitivity}} \underbrace{\left[1 - \left(\frac{T - T_0}{T_m - T_0}\right)^m\right]}_{\text{Thermal softening}} . \quad (10)$$

Here, σ_{eq} is flow stress, A, B, C, n, m are material constants. Furthermore, ε_p is the equivalent plastic strain, $\dot{\varepsilon}_p$ is the plastic strain-rate, $\dot{\varepsilon}_0$ is a reference strain-rate, T_m is the melting temperature, and T_0 is a reference temperature.

In addition to the constitutive material model, Johnson-Cook damage model is used by Mandaj et.al. to simulate failure and is given by,

$$\varepsilon_f = \underbrace{[D_1 + D_2\exp(D_3\sigma^*)]}_{\text{Pressure dependence}} \underbrace{[1 + D_4\ln|\dot{\varepsilon}^*|]}_{\text{Strain rate}} \underbrace{[1 + D_5T^*]}_{\text{Temperature}} . \quad (11)$$

Here, ε_f is the equivalent fracture strain and $D_1 - D_5$ are material constants. Fracture occurs when the cumulative equivalent plastic strain equals ε_f. The damage of an element, D is defined based on a cumulative damage law, represented by,

$$D = \sum \frac{\Delta\varepsilon_p}{\varepsilon_f} . \quad (12)$$

D equals unity signifies fracture. The stress tensor in the material undergoing deformation is given by the scalar damage equation,

$$\sigma_D = (1 - D)\sigma_{eq} . \quad (13)$$

It is noteworthy that the particles reaching equivalent fracture strain are deleted from the SPH calculations. But, the mass and energy of these particles are retained. This ensure the conservation of mass and momentum. This is contrary to FEM, where the elements are completely deleted due to high distortion.

2.4 Calculation cycle

A typical SPH calculation cycle [14] is shown in Fig 2. After the initialization, consisting of domain discritization, assigning material properties and boundary conditions, the conservation equations along with constitutive equations are solved by an explicit time integration using Leap Frog algorithm. Bucket sort algorithm is used for the neighbourhood search.

3 Model description

Turning operation is three dimensional in nature. However, it is simplified to two dimensions with plane strain assumption when the depth of cut, denoted by a_p, is much bigger than the uncut chip thickness, denoted by f. This simplification reduces the computational time of the simulation significantly. Figure 3 shows the zone of simulation for the 2D model.

The model parameters for both the models are chosen according to Mandaj et al. [10], so that there is no need of experiment (the result of SPH model is already compared with the experiment) and the simulation result of models can be compared.
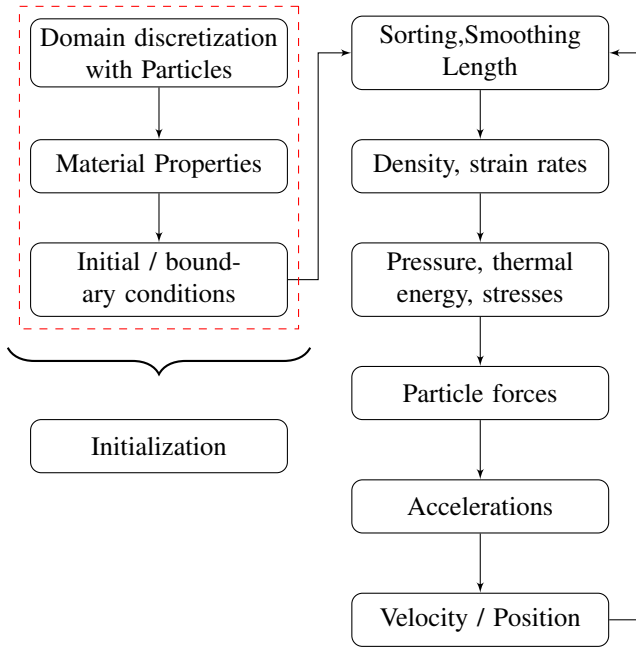
FIGURE 2. The calculation cycle of SPH.
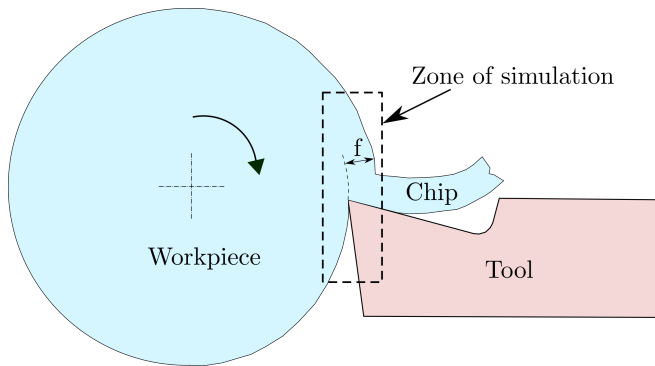
FIGURE 3. 2D simplification of Turning operation

The workpiece dimensions are 5.8 mm × 1.0 mm × 0.05 mm. Tool rake angle is 17.5°, clearance angle is 7° and tip radius of 20 μm. The depth of cut (a_p) is 4 mm and the uncut chip thickness (f) is 0.4 mm.

3.1 The SPH model

The SPH model considered consists of the workpiece discretized completely by particles and the tool by FE elements. The SPH particles are equispaced in all the directions with an inter-particle spacing of 0.025 mm. This leads to a total of 18,560 SPH particles representing the workpiece. The SPH model is shown in Fig. 4. The particle spacing leads to only two layers in the

z-direction. However, since the particles are constrained from moving in the z-direction, the number of layers in z-direction is not relevant to the results of this investigation.

3.2 The SPH-FE coupled model

In the SPH-FE coupled model, the workpiece is divided into two parts. The upper part, where the deformation is high and cutting takes place, is modelled with SPH particles. The lower part is meshed with FEM elements. With this modification, the number of SPH particles decreases by around 50% to 8,816. The SPH-FE coupled model is shown in Fig. 5. The coupling of SPH particles with FE mesh is done by constraining the bottom layer of SPH particles with FE mesh by using the node to surface constraining algorithm. Here, the SPH elements are considered as slave part and the finite elements are considered as master part. The acceleration of each slave node is then interpolated from the master segment containing its contact points [14]. Also, for proper coupling, three rows of SPH elements are kept between the FE mesh and uncut part of SPH elements. This is based on the recommendations by LS-DYNA expats.
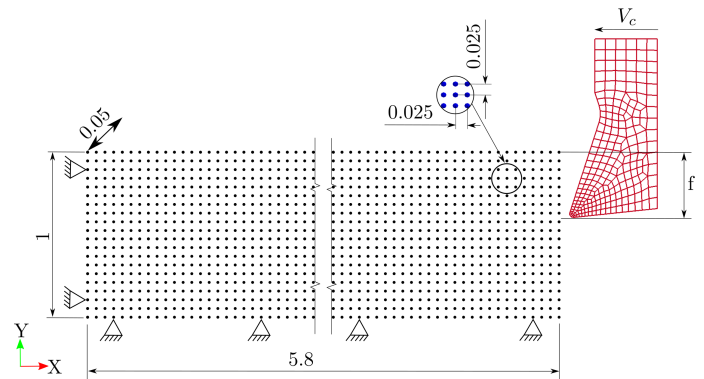
FIGURE 4. The SPH model.
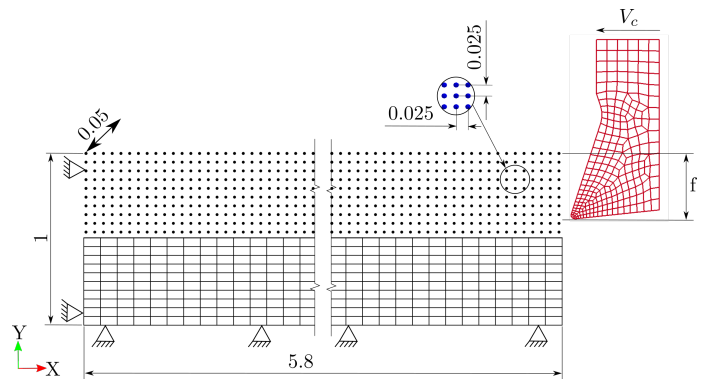
FIGURE 5. The coupled SPH-FE model.

5

TABLE 1. Physical properties of Workpiece and Tool [15].

Property	Workpiece	Tool
Density, ρ (kg/m^3)	2700	11900
Young's Modulus, E (GPa)	73	534
Poisson's ratio, μ	0.33	0.22
Specific heat, C_p (J/Kg K^{-1})	875	-
T_{melt}, (K)	793	-
T_{room}, (K)	300	300

TABLE 2. Johnson-Cook parameters of workpiece (A2024-351) [15].

Parameter	A (MPa)	B(MPa)	n	C	m
Value	352	440	0.42	0.09	1.03
Parameter	D1	D2	D3	D4	D5
Value	0.13	0.13	-1.50	0.011	0

3.3 Boundary conditions

For both the models, the tool is given the cutting velocity of 800 m/min in the negative *x*-direction and completely constrained in all the other directions. The workpiece is fully constrained on the left and bottom sides. Note that for the SPH-FE coupled model, the boundary condition is applied on FEM elements and SPH particles. For plane strain assumption, the motion of all the SPH particles and FEM elements of workpiece and tool is fully constrained in the z-direction (normal to the plane).

3.4 Material model and properties

The workpiece material is aluminium alloy A2024-351 and the tool material is made of an uncoated cemented carbide. The physical properties of workpiece and tool are given in Table 1. The workpiece is modelled using Johnson-Cook material model with Johnson-Cook damage model, given in Table 2. The tool is considered as rigid.

4 Result

All the results shown in the following are for the time when cutting is complete.

4.1 Chip formation

The chip formation for the SPH model and SPH-FE coupled model is shown in Fig. 6 for four different times. The top row of figures correspond to the SPH model and the bottom row corresponds to the SPH-FE model. The chip shape of the SPH model is consistent is with that obtained in [10]. Furthermore,
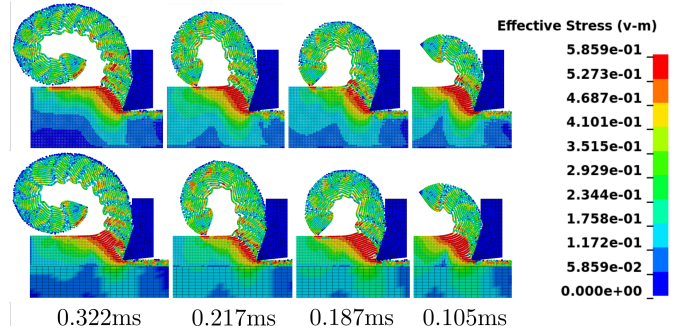
FIGURE 6. Chip shape at four different times as predicted by the SPH and SPH-FE models. The top row represents the SPH predictions whereas the bottom row corresponds to the SPH-FE model.

the chip shape predicted by the SPH-FE model is the same as that predicted by the SPH model at all the four times. The figure also illustrates the ability of SPH method to simulate large deformations occurring during the machining operations. The chip separation, chip curl and self-contact (and highly distorted meshes) are major challenges in Lagrangian FE formulations but easily handled by the SPH method.

Figures 7 and 8 show the distribution of von Mises stress and plastic strain respectively for the SPH model. Again, the results shown in these figures are consistent with [10]. The von Mises stress and plastic strain distribution for the coupled SPH-FE model are shown in Figs. 10 and 11 respectively. Clearly, these results are almost identical to those from the SPH model. Furthermore, it may be observed from these figures that the smoothness of stress distribution across the interface validates the proper coupling between SPH particles and FEM elements.

Another field variable of importance is the damage parameter *D*. In Figs. 9 and 12, the damage variable (*D*) contour plots are provided for SPH model and coupled SPH-FE model respectively. The results match with each other. Moreover, direct correspondence between the plastic strain plot Fig. 8 and damage variable Fig. 11 can be observed. The damage variable is close to unity for the region where plastic strain is more than 0.65 (value of ε_f used in [10]).

4.2 Cutting force

Finally, in Fig. 13, the cutting force predictions are compared. The average cutting force predicted by the SPH model is 904 N whereas it is 911 N for the coupled SPH-FE model. Thus, based on these observations, it is clear that the two models provide essentially the same results although in the SPH-FE problem, the number of SPH particles is around 50% less than that in the SPH model.
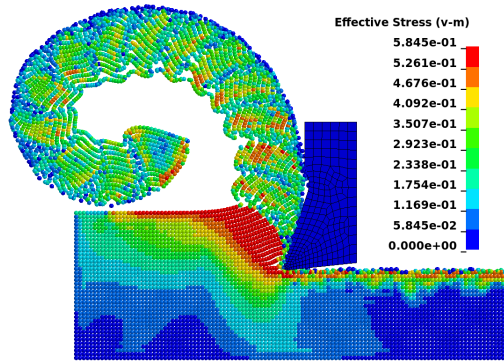
FIGURE 7. von Mises stress distribution for the SPH model.
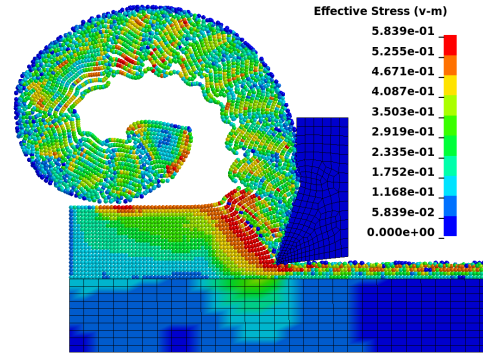
FIGURE 10. von Mises stress for coupled SPH-FE model.
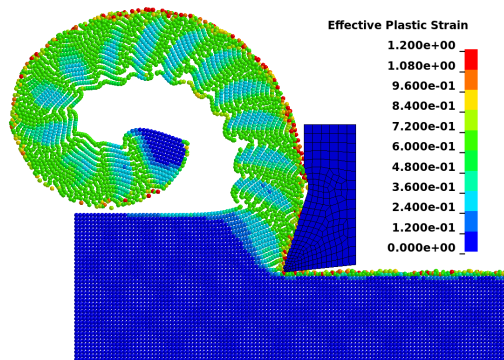
FIGURE 8. Plastic strain distribution predicted by the SPH model.
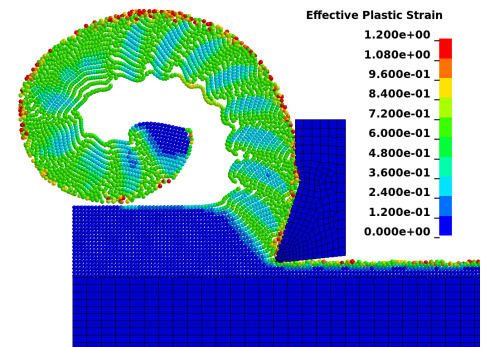
FIGURE 11. Plastic strain distribution for coupled SPH-FE model.
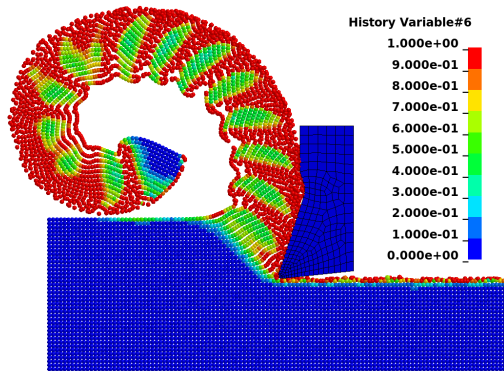
FIGURE 9. Damage variable (D) for SPH model
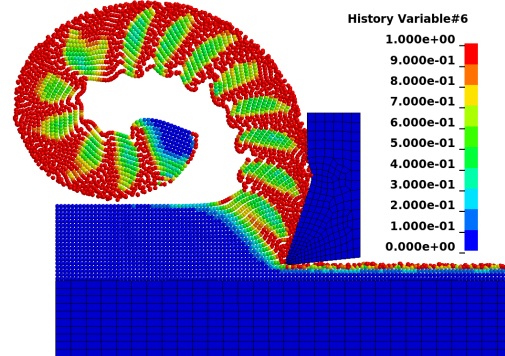
FIGURE 12. Damage variable (D) for SPH-FE coupled model.

4.3 Simulation time

The SPH-FE model took approximately 77 minutes whereas the SPH model took approximately 144 minutes. Clearly, the SPH-FE model offers the advantage of faster run times while predicting results almost identical to the SPH model. This benefit in computation time is because of reduction in number of SPH particles in the model and also the reduction in the contact domain size

of SPH particles in the model. Thus, it may be concluded that the more realistic simulations of machining operations including three-dimensional simulations of cutting can be be performed without loss of much accuracy by using the coupled SPH-FE models while retaining the benefits that SPH method has for machining operations.
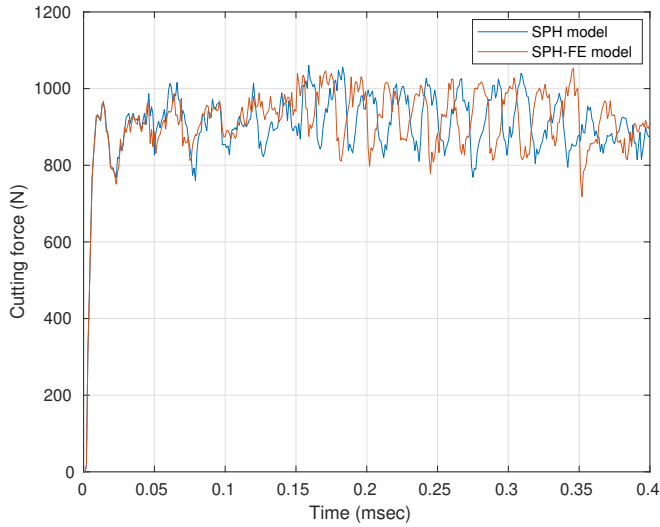
FIGURE 13. Cutting force evolution with time.
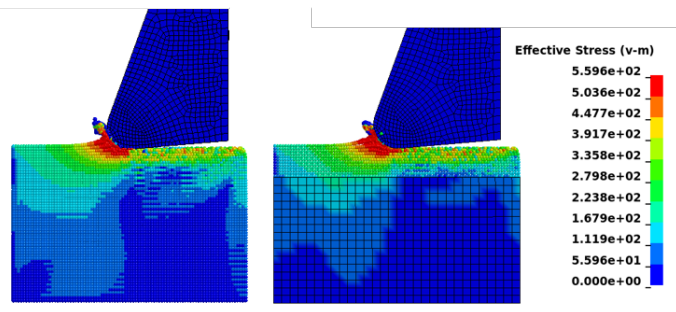
FIGURE 14. von Mises stress distribution.

4.4 Application to Micro-cutting

The approach of coupling SPH and FE is also applied to the micro-cutting of OFHC copper. The model parameters for both the models are chosen according to Zhao et al. [16]. Figure 14 shows the distribution of von Mises stress for the SPH model and coupled SPH-FE model. The results match with each other. Also, the cutting force is 15 N for SPH model vs 15.1 N for the coupled SH-FE model. However, there is 43% reduction in the computation cost.

5 Discussion

The SPH-FE coupling has been used by various researchers for applications like metal machining [11], bone cutting [17] and hyper-velocity impact [18], [19]. The conclusion of these studies is that the SPH method is more accurate for the high deformation applications. However, to the author's knowledge, no direct study for comparing the result of the SPH method and the coupled SPH-FE model for the machining application has been done.

TABLE 3. Simulation time with mesh refinement

Test case	SPH	FE	Time (min)
Coarse SPH	18560	687	144
Refined SPH	62640	687	971
Coarse coupled SPH-FE	9280	1267	77
Refined coupled SPH-FE	31320	1267	522

In line with the result in [19], the computation time increases drastically with the mesh refinement of SPH particles, as shown in Table 5. Calculation of interaction of particle with its neighbour is the major contributing factor [13]. This drastic increase in computation time with the mesh refinement clearly suggests for the use of the coupled SPH-FE method.

Another advantage of using the coupled SPH-FE model is that it reduces the zone of SPH, leading to less increase in the number of SPH particles on mesh refinement. This is because of the fact that the mesh refinement for the SPH is done in all three dirctions, as the accuracy of the SPH method depends on the uniform distribution of SPH particles [20].

6 Conclusion

In this study, a comparison of two simulation models, namely SPH model, with workpiece completely modelled by SPH particles and coupled SPH-FE model, with workpiece modelled by SPH particles and FE mesh, is done to simulate the machining of aluminium alloy A2024-351 and the micro-cutting of OFHC copper. The chip profile, von Mises stress and plastic strain match closely. The reduction of 40% in simulation time is the advantage of the coupled SPH-FE model. This becomes important given the fact that SPH simulations are computation expensive. This benefit becomes more significant for modeling three-dimensional machining problems efficiently.

REFERENCES

[1] Zhang, B., and Bagchi, A., 1994. "Finite element simulation of chip formation and comparison with machining experiment".

[2] Carroll III, J. T., and Strenkowski, J. S., 1988. "Finite element models of orthogonal cutting with application to single point diamond turning". *International Journal of Mechanical Sciences, **30**(12), pp. 899–920.*

[3] Movahhedy, M., Gadala, M., and Altintas, Y., 2000. "Simulation of the orthogonal metal cutting process using an arbitrary lagrangian–eulerian finite-element method". *Journal of materials processing technology, 103*(2), pp. 267–275.

[4] Gingold, R. A., and Monaghan, J. J., 1977. "Smoothed particle hydrodynamics: theory and application to non-spherical stars". *Monthly notices of the royal astronomical society, 181*(3), pp. 375–389.

[5] Limido, J., Espinosa, C., Salaün, M., and Lacome, J.-L., 2007. "SPH method applied to high speed cutting modelling". *International journal of mechanical sciences, 49*(7), pp. 898–908.

[6] Espinosa, C., Lacome, J.-L., Limido, J., Salaün, M., Mabru, C., and Chieragatti, R., 2008. "Modelling High Speed Machining with the SPH Method".

[7] Schwer, L. E., and Windsor, C., 2009. "Aluminum plate perforation: a comparative case study using Lagrange with erosion, multi-material ALE, and smooth particle hydrodynamics". In Seventh European LS-DYNA Conference, Stuttgart, Germany, June, Vol. 10.

[8] Villumsen, M. F., and Fauerholdt, T. G., 2008. "Simulation of metal cutting using smooth particle hydrodynamics". *LS-DYNA Anwenderforum, C-III, 17*.

[9] Avachat, C. S., and Cherukuri, H. P., 2015. "A parametric study of the modeling of orthogonal machining using the smoothed particle hydrodynamics method". In ASME 2015 International Mechanical Engineering Congress and Exposition, American Society of Mechanical Engineers Digital Collection.

[10] Madaj, M., and Píška, M., 2013. "On the SPH orthogonal cutting simulation of A2024-T351 alloy". *Procedia Cirp, 8*, pp. 152–157.

[11] Xi, Y., Bermingham, M., Wang, G., and Dargusch, M., 2014. "SPH/FE modeling of cutting force and chip formation during thermally assisted machining of Ti6Al4V alloy". *Computational materials science, 84*, pp. 188–197.

[12] Feng, L., Liu, G., Li, Z., Dong, X., and Du, M., 2019. "Study on the effects of abrasive particle shape on the cutting performance of Ti-6Al-4V materials based on the SPH method". *The International Journal of Advanced Manufacturing Technology, 101*(9-12), pp. 3167–3182.

[13] Liu, G., Liu, M., and Li, S., 2004. "Smoothed particle hydrodynamics—a meshfree method". *Computational Mechanics, 33*(6), pp. 491–491.

[14] Jo, H., 2006. "LS-DYNA theory manual". *LSTC, Livermore-California*.

[15] Mabrouki, T., Girardin, F., Asad, M., and Rigal, J.-F., 2008. "Numerical and experimental study of dry cutting for an aeronautic aluminium alloy (A2024-T351)". *International Journal of Machine Tools and Manufacture, 48*(11), pp. 1187–1197.

[16] Zhao, H., Liu, C., Cui, T., Tian, Y., Shi, C., Li, J., and Huang, H., 2013. "Influences of sequential cuts on micro-cutting process studied by smooth particle hydrodynamic (sph)". *Applied surface science, 284*, pp. 366–371.

[17] Li, S., Zahedi, A., and Silberschmidt, V., 2018. "Numerical simulation of bone cutting: Hybrid sph–fe approach". In *Numerical methods and advanced simulation in biomechanics and biological processes*. Elsevier, pp. 187–201.

[18] Swaddiwudhipong, S., Islam, M., and Liu, Z., 2010. "High velocity penetration/perforation using coupled smooth particle hydrodynamics-finite element method". *International Journal of Protective Structures, 1*(4), pp. 489–506.

[19] Azevedo, R. L., and Alves, M., 2009. "Numerical simulation of soft-body impact on gfrp laminate composites: mixed sph-fe and pure sph approaches". *Mechanics of solids in Brazil*, pp. 15–30.

[20] Liu, M., and Liu, G., 2010. "Smoothed particle hydrodynamics (sph): an overview and recent developments". *Archives of computational methods in engineering, 17*(1), pp. 25–76.